Pretransitional nematic ordering in liquid crystals with dispersed polymer networks

Y. K. Fung,[1,*] A. Borštnik,[2] S. Žumer,[2] D.-K. Yang,[1] and J. W. Doane[1]
[1]*Liquid Crystal Institute, Kent State University, Kent, Ohio 44242*
[2]*Department of Physics, University of Ljubljana, Jadranska 19, 1000 Ljubljana, Slovenia*
(Received 15 July 1996)

The birefringence induced by partially ordered polymer networks dispersed in an isotropic phase of liquid crystals is studied. Polymer networks were formed by the polymerization of 1–4 % mixtures of prepolymer in the nematic phase of liquid crystals. The partial nematic (paranematic) ordering is analyzed in terms of the Landau–de Gennes approach using a simple model of an array of thin fibrils, which can, on a large scale, form bundles of polymer-rich material. The comparison of the theory and birefringence data clearly shows that the main building bloc of the network is a few nanometers thick fibril. The average thickness of fibrils varies slightly with the polymer concentration. The information obtained on large scale (micrometer) structures is not conclusive and must be complemented by other methods. The network on the average retains 30–50 % of the order parameter of the environment where it was formed. [S1063-651X(97)12202-4]

PACS number(s): 61.30.−v, 42.70.Df, 64.70.Md, 61.25.Hq

I. INTRODUCTION

Low concentration polymer networks, which are capable of capturing the orientational order of the nematic liquid crystal environment where they are assembled, exhibit several interesting physical phenomena [1–5]. These composite materials are becoming particularly attractive because of their potential for use in a variety of new electro-optic technologies [6]. The best known examples are the normal and reverse mode light shutters [7], bistable reflective mode display [8–10], volume-stabilized ferroelectric and antiferroelectric liquid crystal displays [11], and modified twisted-nematic displays [12,13].

These materials have many physical properties analogous to liquid crystals confined to well-defined submicrometer-sized spherical and cylindrical cavities [14,15] and random porous matrices [16–20]. Because of its large surface-to-volume ratio, polymer networks strongly influence nematic ordering in the liquid crystalline background on micrometer and nanometer scales and thus govern optical properties of the composite.

The currently available information about these systems was inferred from electron microscopy [21–23], birefringence [22], dichroism [4], and dielectric spectroscopy [24] in dispersions of high polymer concentration, and from magnetic resonance [25], diamagnetic and viscosity measurements [26], birefringence [2], small angle neutron scattering measurements [3], and nuclear magnetic relaxation [27] in low concentration dispersions. Although the evidence about structures on micron and submicron scales is rather conclusive, there are only preliminary results [2,27] showing that networks are strongly distributed on the nanometer scale. For more details on related materials, see relevant chapters in Ref. [28].

In this paper, we focus our attention on a surface-induced orientational ordering at temperatures above the nematic-isotropic phase transition. To describe this partial nematic ordering, we use the term ''paranematic ordering'' [29]. Similarly as in simple planar [30], spherical [14], and cylindrical [15] geometries, we develop a phenomenological description. We follow our initial efforts [2,31] and show how an improved, although still simple, phenomenological model allows us to describe the pretransitional behavior of the birefringence in these complex systems. In particular, we focus on the structural information which can be obtained by a careful analysis of the experimental data.

II. EXPERIMENTAL RESULTS

Nematic order in the prepolarization state is characterized by the director field and degree of order. It was shown that a structure of a polymer network that was polymerized from monomers of liquid-crystallinelike molecules in a nematic solution, always reflects the initial director field [1,2]. The effective macroscopic degree of order of our system composed of the polymer network and liquid crystal depends on a wide range of scales. In further discussions we shall distinguish between molecular scale ordering and submicrometer scale ordering, denoted *local* and *macro*, respectively.

A. Scanning electron microscopy

Following our previous study [32], we used a scanning electron microscope (SEM) to study the submicrometer structures of polymer network formed in nematic phase. In this experiment, 2 wt % BAB6{4,4′-bis[6-(acryloyloxy)-hexyloxy]-1,1′biphenylene} and a very small amount of photo-initiator BME (bezoin methyl ether) (a few percent of the monomer) was mixed with nematic liquid crystal E48 (commercial mixture of cyanobiphenyls). At room temperature in nematic phase, the resulting material was used to fill a 10 μm-gap cell, and then exposed to UV light for photopolymerization. During the polymerization, an external electric field was applied to the cell to ensure a homogeneous homeotropic state of the liquid crystal. After the polymerization, we first removed the seal on the cell, and immersed the

*Present address: Varitronix Limited, 4/F, Liven House, 61-63 King Yip St., Kwun Tong, Kowloon, Hong Kong.

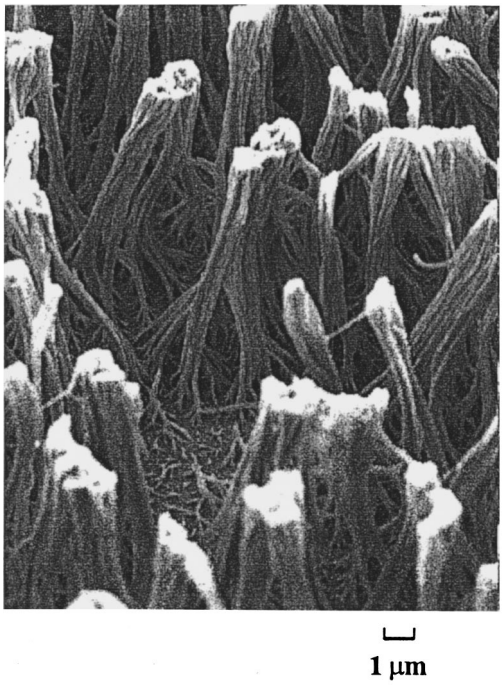

FIG. 1. Polymer network originally formed in a homeotropically oriented liquid crystal and examined with an electron microscope after removal of the liquid crystal.

cell in hexane. Hexane diffused into the cell slowly and replaced the liquid crystal. The cell was placed in a vacuum chamber to allow hexane to evaporate. The cell was opened and the polymer network left on the glass substrate was examined by SEM. As shown in Fig. 1, a fiberlike polymer network perpendicular to the substrate was observed. The thickness of fibers and aggregates of fibers ranges from 0.1 to 1 μm. Although it was previously claimed [2] that replacement of the liquid crystal with the solvent hexane does not affect the network, this is certainly not true for the evaporation of the solvent. The rather dense SEM-detected structures were the result of shrinking and partial collapse of the network after the solvent was removed. The fact that the structure close to the surface, was less affected by the drying process indicates that fibers of thickness $\sim$0.1 μm after evaporation combine in thicker tree-trunk-like structures. We believe that the fiber structure on the micrometer scale with relatively large interfiber spacings is relevant for electro-optic properties of these materials, but it is not directly related to the network structure on the nanometer scale. Although one can say that an anisotropic polymer network is formed because of the aligning effect and anisotropic diffusion property of the liquid crystal, a more detailed judgement cannot be made without detailed insight in the ordering on the molecular scale. Therefore, we decided to perform the precise birefringence study described below.

B. Measurements of optical anisotropy

We studied the polymer-network-induced birefringence of a nematic liquid crystal in the isotropic phase. In this experiment, monomer BMBB-6(4′4-bis-{4-[6-(methacryloyloxy)-hexyloxy]benzoate}-1,1′biphenylene) and a very small amount of photoinitiator BME were mixed with 5CB (4-pentyl-4 cyanobiphenyl). Mixtures with 1, 2, 2.5, 3, and 4 wt % of monomer were prepared in the nematic phase at room temperature. Concentrations were controlled within relative error 10^{-2}. Mixtures were poured into planar cells with the gap controlled by 29- μm mylar film. The cells had rubbed polyamide surfaces and the nematic in the cells had a homogeneous planar alignment. To achieve a reproducible photopolymerization, all cells were irradiated by UV light (4 W/cm^2) at constant ambient temperature for one hour. After the polymerization, each cell was used for the birefringence study with the light of a He-Ne laser. The polarizer and analyzer were crossed, and the cell was aligned such that the rubbing direction (director field $\hat{n}$) was at 45° to the polarizer and analyzer. The light beam was normal to the cell and the transmitted light intensity was measured as a function of temperature with a 10-mK precision.

The intensity of the transmitted light is described by

$$I = I_0 \sin^2(\delta/2), \tag{1}$$

where δ is the phase shift between the ordinary and extraordinary components of light given by $2\pi\Delta n d/\lambda$ with Δn as the effective birefringence and d as the relevant thickness of the layer. This equation allows us to determine within a few % precision the temperature dependence of the effective birefringence for our samples.

1. Isotropic network in a liquid crystal phase

The UV photopolymerization performed in the isotropic phase results in a polymer network exhibiting high light-scattering when cooled to the nematic phase, but it was completely black when put between crossed polarizers and viewed above the nematic-isotropic transition temperature (T_{Ni}). This experiment reveals that the polymer network assembled in the isotropic phase does not posses any long-range order. Such a situation prevents us from using birefringence measurements for a local-order study. If there is a local order, its range is small compared to the wavelength of light. Therefore, its effect is completely averaged out by a light beam sampling randomly oriented areas of local order.

2. Ordered network in an isotropic liquid crystal

The pretransitional increase of the effective birefringence shown in Fig. 2(a) as a function of temperature for 1%, 2%, 2.5%, 3%, and 4% concentrations of the BMBB6-based network, is very strong. This suggests that in addition to the contribution of the polymer network assembly, there is a temperature-dependent contribution from the paranematic order induced in the isotropic liquid crystal phase by the internal surfaces of the polymer network.

3. Ordered network in an isotropic solvent

To decipher the relative contributions to the net birefringence of the polymer network and the surface-induced order, we replaced the liquid crystal, which surrounds the network, with the isotropic fluid chlorobenzene. Since the chlorobenzene molecules are too ''spherical'' to expect any ordering at the polymer network surfaces, the birefringence can be attributed solely to the polymer network assembly. Applying the same method to measure the birefringence of the polymer

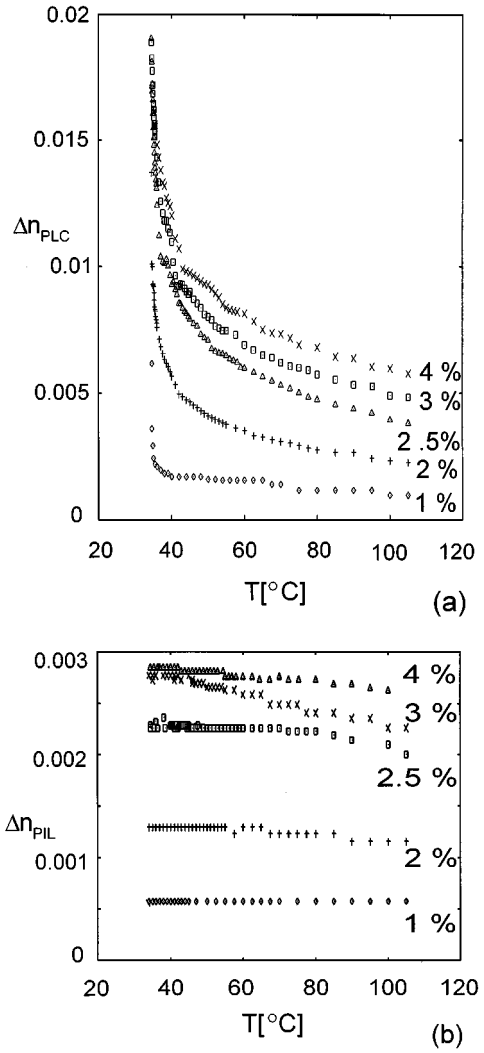

FIG. 2. Experimentally determined temperature dependence of birefringency of a (a) polymer network in an isotropic liquid crystal, (b) polymer network in an isotropic solvent for several polymer concentrations.

network assembly in the isotropic solvent (Δn_{PIL}), Δn_{PIL} was estimated to be between 5×10^{-4} and 3×10^{-3}, depending on the network concentration η [see Fig. 2(b)]. The weak temperature dependence indicates that networks are rigid and stable up to 100 °C. As no appreciable change in the volume of the network was detected when the liquid crystal was replaced with the chlorobenzene, one can assume that the effective order parameter of the network is also the same as when being dispersed in the liquid crystal matrix.

III. MODEL STRUCTURE OF THE NETWORK

Following our previous paper [2], the polymer network dispersed in a liquid crystal is approximated by an array of thin polymer fibrils. As the polymer network grows in a nematic liquid crystal, we expect that fibrils are formed along the local director field. We described them locally as parallel cylindrical rods characterized by radius R and packed into a two-dimensional square array with interfibrile distance d [Fig. 3(a)]. The space between the polymer fibrils is filled with a liquid crystal. The monomers—constituting

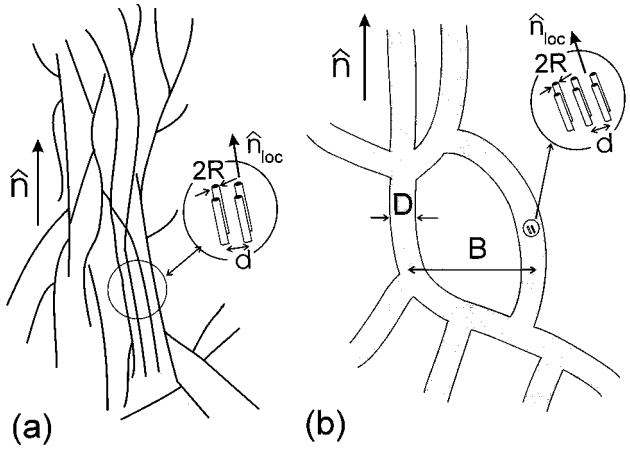

FIG. 3. Schematic presentation of the polymer network in (a) one-scale (fibril) and (b) two-scale (fibril-bundle) model showing both local and macro director. In both cases, the local distribution of fibrils is represented by a square array of polymer fibrils. The relevant distances are also illustrated.

units of the network—have a chemical structure similar to liquid crystal molecules. Therefore, we assume that both densities are similar and all concentrations can be directly related to the ratios of the occupied volumes. The local order parameter Q_p of the polymer network is also assumed to be equal to the order parameter Q_n of the bulk nematic liquid crystal where it was formed. Further, we assume that polymer-induced paranematic order is uniaxial with the director $\hat{n}_{\mathrm{loc}}$ parallel to the polymer fibrils. This allows us to describe the paranematic ordering in the interfibril space by a simple scalar order parameter field $Q(\vec{r})$ [33]. Once R is chosen, using geometrical considerations, d follows from the concentration $\eta=\pi R^2/d^2$. Such a single scale model is expected to be useful for the description of the paranematic ordering in the isotropic phase with very low concentrations of polymer, where local effects are dominant. On the contrary, in the nematic phase, because of the elastic deformation energy, long-range effects are dominant also in the case of low polymer concentration. To take into account the observations [23,32,26,3], indicating the existence of fiberlike objects with diameters around 0.1 μm, we assume that thin fibrils form bundles of polymer-rich material where concentration $\eta'=\pi R^2/d^2$ is larger than the average polymer concentration η. Let us assume a bundle to be parallel cylinders with typical diameter D forming a large (micrometer)-scale network, here, simply represented by an average interbundle distance B [Fig. 3(b)]. To be able to estimate the effect of such two-scale structures, we will simply represent the network distribution by another regular square array of parallel bundles characterized by interbundle distance B. In the space between bundles, the polymer concentration is low and thus does not contribute to the paranematic ordering. It should be stressed that in the nematic phase, the behavior of these parts of liquid crystal is characterized by constraints on the scale of interbundle distance B, while the behavior of the liquid crystal in the bundles is characterized by the much smaller interfibrile distance d. Therefore, only liquid crystal in the polymer-poor regions can be easily affected by an applied electric field and is thus useful for the electro-optic applications. This fibril-bundle picture will be denoted as a two-

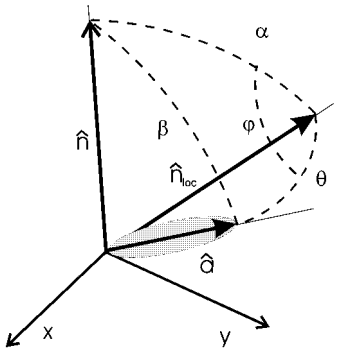

FIG. 4. Schematic presentation of the macro director $\hat{n}$, local director $\hat{n}_{\rm loc}$, and unit vector $\hat{a}$, which denotes the directions of the long axes of a molecule. The relevant angles are shown as well.

scale model of the polymer network.

On the macro scale, the polymer network (in the single- or two-scale model) is disordered in addition to the local-scale disorder of the polymer forming fibrils. Therefore, it is useful to introduce the macro director $\hat{n}$, and local director $\hat{n}_{\rm loc}$ [see Fig. 3]. Further, also angles α, β, θ, and φ related to the orientations of a molecular vector $\hat{a}$, macro director $\hat{n}$, and local director $\hat{n}_{\rm loc}$ are introduced (see Fig. 4). Using the trigonometrical relation $\cos^2\beta=\cos^2\alpha\cos^2\theta+\sin^2\alpha\sin^2\theta\cos^2\varphi$ and assuming that the global average $\langle\ \rangle$ can be separated in the two independent averages one $\langle\ \rangle_{\rm loc}$ over local variables φ and θ and second $\langle\ \rangle_{\rm macro}$ over macro variable α, the global order parameter can be written as

$$\tfrac{1}{2}\langle 3\cos^2\beta-1\rangle=\tfrac{1}{2}\langle 3\cos^2\alpha-1\rangle_{\rm macro}\tfrac{1}{2}\langle 3\cos^2\theta-1\rangle_{\rm loc}. \tag{2}$$

Using the notation $\langle Q_{\rm pol}\rangle$ for the global order parameter of the network alone, $Q_{\rm macro}$ for the macro order parameter, and the above assumption for the local polymer order to be equal to Q_n, the Eq. (2) can be written as

$$\langle Q_{\rm pol}\rangle=Q_{\rm macro}Q_n. \tag{3}$$

Thus, an experimental determination of $\langle Q_{\rm pol}\rangle$ will directly give the value of $Q_{\rm macro}$.

In case of the liquid crystal order parameter, we have also non-negligible spatial variation of the paranematic order. Therefore, in the definition of the average local order parameter $\frac{1}{2}\langle 3\cos^2\theta_{\rm LC}-1\rangle_{\rm loc}=Q$ is introduced to stress the spatial averaging. So the product

$$\langle Q_{\rm LC}\rangle=Q_{\rm macro}\overline{Q} \tag{4}$$

will be used for the average order parameter of the liquid crystal. In the next section, Q will be calculated for the above geometrical models, assuming that the polymer surface induces paranematic ordering characterized by the surface preferred value Q_n and an unknown coupling strength G.

Summarizing, we can stress that in the one-scale model we will have two fitting parameters (R,G) and the relation $\eta=\pi R^2/d^2$. In the two-scale model for the description of ordering, two additional parameters (D,B) are needed. To reduce the freedom, the bundle thickness D will be taken to be 60 nm using the results of Jakli *et al.* [26,3], which is also in agreement with our SEM study. Further, we shall use the ratio of the polymer concentration in the bundle (η') to the average concentration (η) $\eta'/\eta=B^2/[\pi(D/2)^2]$ as a parameter instead of the interbundle distance B. One should also have in mind that here, $\eta'=\pi R^2/d^2$. Thus, our fitting procedure for the two-scale model will take into account the independent parameters $(R,\ \eta'/\eta,\ G)$.

IV. OPTICAL ANISOTROPY

A. Nonuniform composite system

Macroscopic birefringence of a material composed of anisotropic molecules is caused by their long-range orientational order. In a composite system, there are contributions arising from all components. The anisotropy of the dielectric tensor is in the uniaxial medium proportional to the orientational order parameter Q, while for the birefringence $\Delta n\propto Q$ is realized only in the limit $\Delta n\ll n$ [33]. In our case of a polymer dispersion in an isotropic liquid or isotropic phase of the liquid crystal, this limit is very well justified. If Δn_0 stands for the birefringence of a perfectly orientationally ordered homogeneous material with $Q=1$, the birefringence is simply given by $\Delta n=Q\Delta n_0$.

The situation is more complicated when a light beam passes through a sample with nonuniform direction and degree of ordering or a composite system where light is refracted and scattered. The refraction is linear in the order parameter and is thus expected to be crucial in the case of small variations. The scattering effects are quadratic in order parameter variations and strongly dependent on the scale of the spatial variations in the order parameter.

To estimate the relevance of light scattering, let us first assume that the sample consists of domains with size $D\ll\lambda$. Using a Raleigh or Raleigh-Gans description [34], the scattering cross section of such a domain can be approximately written as $\sigma\sim(\Delta n_0Q)^2D^6/\lambda^4$. Taking D^{-3} for the density of randomly oriented domains and following Žumer *et al.* [35], one can estimate the extinction coefficient as $\sigma/D^3\sim(\Delta n_0Q)^2D^3/\lambda^4$. For small domains, $D\leqslant 0.1\lambda$, the extinction coefficient is negligible even in a nematic liquid crystal phase, where $\Delta n_0Q\sim 0.2$ yields $\sigma/D^3\sim<10^{-4}\ \mu{\rm m}^{-1}$. The scattering of the domains with $D\sim\lambda$ can be treated using anomalous diffraction approximation [34]. One can estimate the cross section of such a domain as $\sigma\sim(\Delta n_0Q)^2D^4/\lambda^2$ and, as above, the corresponding extinction coefficient: $\sigma/D^3\sim(\Delta n_0Q)^2D/\lambda^2$. For a layer of thickness h with inhomogeneities on the length scale $D=\lambda$, the relative amount of the transmitted light $I_{\rm trans}$ is approximately given by $\exp[-(\Delta n_0Q)^2h/\lambda]$. A crossing of the $T_{\rm NI}$ transition point in case of the μm layer yields the reduction of the exponent from ~ 1 to $\sim 10^{-2}$. This explains strong light scattering in the nematic phase and practically no scattering in the isotropic phase. Therefore, in our discussion of the optical anisotropy in the paranematic phase of the composite, where liquid crystal and polymer components are relatively well dispersed on the scale comparable to the wavelength of visible light, the scattering phenomena can be neglected.

The effective birefringence is thus simply given by an average over the space of the order parameter:

$$\Delta n = \frac{1}{V}\int_V \Delta n_0 Q(\vec{r}) d^3 r, \tag{5}$$

where V is the volume sampled by the beam used in probing birefringence. Because we have two components, we can write

$$\Delta n = \Delta n_{0\mathrm{LC}} \frac{1}{V}\int_{V_{\mathrm{LC}}} Q(\vec{r}) d^3 r + \Delta n_{0\mathrm{pol}} \frac{1}{V}\int_{V_{\mathrm{pol}}} Q(\vec{r}) d^3 r, \tag{6}$$

where $\Delta n_{0\mathrm{LC}}$ and $\Delta n_{0\mathrm{pol}}$ are indices of completely oriented liquid crystal and polymer, respectively. Assuming that densities of both materials do not differ much, we can introduce $\eta = V_{\mathrm{pol}}/V$ as the percentage of the polymer and write

$$\Delta n = (1-\eta)\Delta n_{0\mathrm{LC}} \langle Q_{\mathrm{LC}}(\vec{r})\rangle + \eta \Delta n_{0\mathrm{pol}} \langle Q_{\mathrm{pol}}(\vec{r})\rangle. \tag{7}$$

Using the above descriptions [Eq. (3,4)] for the averaged order parameters and simply taking 1 instead of $1-\eta$, and $\Delta n_{0\mathrm{LC}}$, $\Delta n_{0\mathrm{pol}} = \Delta n_0$ one can write

$$\Delta n = \Delta n_0 Q_{\mathrm{macro}}[\overline{Q(G,Q_n)} + \eta Q_n] \tag{8}$$

for the effective index of refraction.

V. ORDER PARAMETER OF THE LIQUID CRYSTAL

Being satisfied with a scalar order parameter, we can follow our approach used for the description of the pretransitional paranematic ordering in submicrometer pores [15]. The simple Landau–de Gennes expression for the free-energy density [36],

$$f = f_0 + \tfrac{1}{2}a[T-T^*]Q^2(\vec{r}) - \tfrac{1}{3}bQ^3(\vec{r}) + \tfrac{1}{4}cQ^4(\vec{r}) + \tfrac{3}{4}L_1[\vec{\nabla}Q(\vec{r})]^2 + G[Q(\vec{r})-Q_n]^2\delta(|\vec{r}-\vec{r}_{\mathrm{LC-pol}}|), \tag{9}$$

is supplemented by the surface coupling, taking care of the polymer network effect on the ordering of the liquid crystal. The constants $a = 0.13\times10^6$ J/m^3 K, $b = 1.8\times10^6$ J/m^3, $c = 4.1\times10^6$ J/m^3, $T^* = 307$ K, and $L_1 = 1.1\times10^{-11}$ J/m (see Ref. [37]) will be used, while the constant f_0 does not play any role. We use the form of the surface coupling previously applied to porous media [15,38]. At the surface of the polymer fibril, this term tends to equalize the order parameter of the liquid crystal (Q) with the order parameter of the polymer (Q_n). The strength of the coupling is characterized by the constant G. As we mentioned before, the local polymer order parameter is for simplicity taken to be equal to the ''original'' order parameter of the bulk liquid crystal where network was formed.

The order parameter profile of the liquid crystal in the equilibrium state is derived by minimizing the total free energy F of the system and thus setting

$$\delta F = \delta\int_V d^3 r f(Q(\vec{r}), \vec{\nabla}Q(\vec{r}), T) = 0. \tag{10}$$

Applying Eq. (10) to the free-energy density [Eq. (9)], the following second-order differential equation

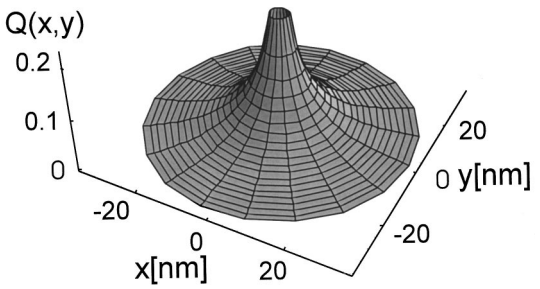

FIG. 5. A three-dimensional plot $Q(x,y)$ of the order parameter of the liquid crystal in the vicinity of a single polymer fiber is shown. Q is a function of the distance from the axes of the polymer fiber only $Q = Q(r)$. The radius of the polymer fiber is equal to $R = 2.5$ nm, the constants $G = 0.011$ J/m^2 and $Q_n = 0.3$, and the temperature $T_{\mathrm{NI}} + 1.62$ K.

$$a[T-T^*]Q(\vec{r}) - bQ^2(\vec{r}) + cQ^3(\vec{r}) - \tfrac{3}{2}L_1\vec{\nabla}^2 Q(\vec{r}) = 0, \tag{11}$$

and the boundary condition at the surface of the polymer fibril

$$\tfrac{3}{2}L_1(\vec{\nabla}Q(\vec{r}))_{|\vec{r}|=R,\perp} - 2G(Q(\vec{r})-Q_n)_{|\vec{r}|=R} = 0, \tag{12}$$

are obtained. The symbol $_\perp$ stands for the direction perpendicular to the surface of the polymer fibril.

We shall treat two samples: a sample in a diluted polymer network limit and a sample in which the distances between the polymer fibrils are comparable to nematic correlation length.

In the case of a very diluted polymer network or at high temperatures, liquid crystal is ordered only in the vicinity of the polymer fibers. We use therefore a single fiber description. The cylindrical symmetry of the polymer fiber suggests the introduction of the cylindrical coordinates with the origin at the symmetry axes of the polymer fibril. In this case, it is meaningful to express the differential equation (11) and boundary condition at the surface of the polymer fibril (12) in cylindrical coordinates

$$a[T-T^*]Q(r) - bQ^2(r) + cQ^3(r) - \tfrac{3}{2}L_1\left(\frac{1}{r}\frac{\partial Q(r)}{\partial r} + \frac{\partial^2 Q(r)}{\partial r^2}\right) = 0,$$

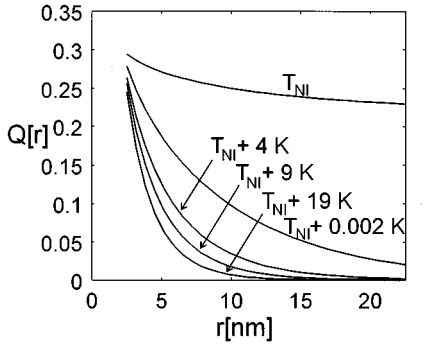

FIG. 6. Order parameter profile $Q(r)$ for different temperatures in the vicinity of the temperature of the phase transition. Parameters are the same as in Fig. 5.

$$\tfrac{3}{2}L_1\left(\frac{\partial Q(r)}{\partial r}\right)_{r=R} - 2G[Q(R)-Q_n]=0. \tag{13}$$

Since the influence of the polymer fibril on the ordering of the liquid crystal that is far away from the surface of the fibril is negligible, we require

$$\left(\frac{\partial Q(r)}{\partial r}\right)_{r\gg R}=0. \tag{14}$$

Since the order parameter Q is a function of the distance from the symmetry axes of the polymer fibril only, we use a one-dimensional relaxation method for solving differential Eq. (13).

In Fig. 5, the three-dimensional presentation of the order parameter $Q(r)$ in the vicinity of a single fibril, calculated using Eq. (13) for the liquid crystal in isotropic phase, is shown. We choose the radius of the polymer fibril $R=2.5$ nm, the constant $G=0.011$ J/m^2, and the temperature $T_{\rm NI}+1.62$ K. Figure 6 presents $Q(r)$ for different temperatures in the vicinity of the phase transition temperature. The order parameter was calculated from Eq. (13) using the relaxation method. The constants R and G have the same values as in Fig. 5. We can see that the temperature of the phase transition of the liquid crystal lies slightly above the bulk transition temperature ($T_{\rm NI}$) in the interval between $T_{\rm NI}$ and $T_{\rm NI}+0.002$ K. We can also see that at higher temperatures the order parameter drops almost exponentially with increasing distance from the polymer fibril.

If the order parameter Q is small, and therefore the quadratic and cubic term in Eq. [13(a)] can be neglected, Eq. (13) has an analytical solution. The solution can be expressed with the modified Bessel functions $K_0(z)$ and $K_1(z)$ as follows [23,31]:

$$Q(r)=\frac{Q_n}{K_0\left[R\left(\frac{a}{3L_1}(T-T^*)\right)^{1/2}\right]+\frac{\sqrt{3L_1a(T-T^*)}}{4G}K_1\left[R\left(\frac{a}{3L_1}(T-T^*)\right)^{1/2}\right]}K_0\left[r\left(\frac{a}{3L_1}(T-T^*)\right)^{1/2}\right]. \tag{15}$$

In the case of concentrated polymer network modeled by the square lattice, it is convenient to express the order parameter of the liquid crystal Q as a function of Cartesian coordinates x and y, and to put the origin of the coordinate system at the symmetry axes of a chosen polymer fiber [39]. The differential Eq. (11) and the boundary condition at the surface of the polymer fiber [Eq. (12)] are expressed in Cartesian coordinates as well:

$$\begin{aligned} &a[T-T^*]Q(x,y)-bQ^2(x,y)+cQ^3(x,y)\\ &\quad-\tfrac{3}{2}L_1\left(\frac{\partial^2Q(x,y)}{\partial x^2}+\frac{\partial^2Q(x,y)}{\partial y^2}\right)=0,\\ &\frac{3L_1}{2R}\left(x\frac{\partial Q(x,y)}{\partial x}+y\frac{\partial Q(x,y)}{\partial y}\right)_{\sqrt{x^2+y^2}=R}\\ &\quad-2G[Q(x,y)-Q_n]_{\sqrt{x^2+y^2}=R}=0. \end{aligned} \tag{16}$$

We use the two-dimensional relaxation method to solve Eq. (16). The order parameter Q is calculated for a quarter of a square region shown in Fig. 7. Because of the symmetry of the problem, the derivative of Q on x and y axes in the direction perpendicular to the x and y axes, respectively, has to be equal to zero. The solution for the total area between four fibrils is then simply a composition of these units.

In Fig. 7 we present a three-dimensional plot of the order parameter $Q(x,y)$ of the liquid crystal surrounded by four polymer fibrils using the same parameters as in Fig. 5, but with interfibril distance equal to $8.9R$ (corresponding to the polymer concentration at only 0.04) and with $T=T_{\rm Ni}+4K$. Figure 8 presents the order parameter profile in direction ρ (characterized by $x=y$ in Fig. 7). The order parameter was calculated using the same constants as in Fig. 7. It can be seen that for thin fibrils ($R=1$ μm) and low polymer concentrations, even well beyond the transition point, the parameter Q in between fibrils is too high for the single-fibril approximation.

VI. COMPARISON OF CALCULATED BIREFRINGENCE WITH EXPERIMENTAL DATA

In this section, we calculate the birefringence of the liquid crystal in the isotropic phase, paranematically ordered by the polymer network. The order parameter of the polymer network $\langle Q_{\rm pol}\rangle$ is estimated from experimentally determined birefringence $\Delta n_{\rm PIL}$ of a polymer network dispersed in a totally isotropic liquid by Eq. (8) using $\Delta n_0=0.3$ and $Q=0$. In the case where the concentration of the polymer network is between 0.01 and 0.04, one finds that $\langle Q_{\rm pol}\rangle$ is between 0.15 and 0.28. The value of $\langle Q_{\rm pol}\rangle$ is substantially less than that of the liquid crystal where it was formed, ($Q_n\sim0.5$ at room temperature), which indicates that a substantial amount of cross linking has occurred. This macro scale disorder is characterized by $Q_{\rm macro}$, that is using Eq. (3) estimated to vary between 0.3 and 0.5 depending on the network concentration. The largest value achieved at 3% concentration indicates that network at lower concentrations is probably too fragile to retain all the order of the initial environment where it was formed. On the other hand, with increasing concentration more cross linking is expected and this certainly leads to the decrease of the network orientational order. This network exhibits much higher order as compared to the BAB type [2]. In our case the network looks as though it is built of more or less oriented fibers, while in the BAB case, the structure looks as though it is built of globules not showing any particular order.

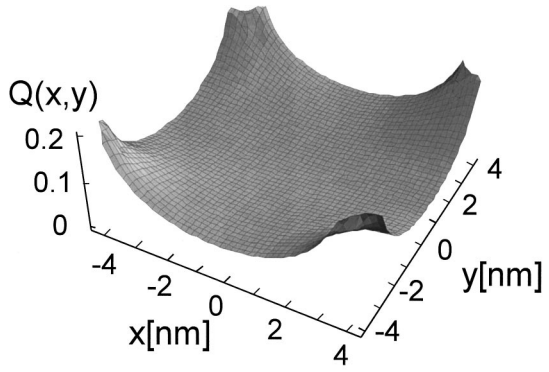

FIG. 7. A three-dimensional plot of the order parameter $Q(x,y)$ of a liquid crystal which is surrounded by four polymer fibrils with radius 1 nm and interfibril distance $d=8.9$ nm. The concentration of the polymer network is equal to 0.04 and the temperature is 4 K above the nematic isotropic transition. Other parameters are the same as in Fig. 5.

The analysis of the combined liquid-crystal–network birefringence is first performed on the above introduced one-scale (fibril) model. For the macro order parameter Q_{macro} obtained from Δn_{PIL}, the paranematic temperature dependence of the birefringence is calculated from Eq. (8) and compared with the experimental data. To cover also the behavior close to the transition temperature, where the single-fibril limit is not applicable, the average Q needed in Eq. (8) is simply obtained for a chosen set of parameters (R,G) by solving the Euler-Lagrange equation (16) for $Q(x,y)$. In order to get the best fit of the calculated birefringence to experimental data, the radius of the polymer fibrils R and surface coupling constant G are varied. In Figs. 9(a) and 9(b), theoretical birefringence is compared with the experimental data for network concentrations 1%, 2%, 2.5%, and 3%. The calculated birefringence is in the best agreement with the experimental data if the radius of the polymer fibers is around 2 nm (1.8, 2, 2.2, and 2.3 nm for concentrations 1%, 2%, 2.5%, and 3%, respectively) and the same surface coupling constant G about 0.01 J/m^2. For 1% concentration of polymer fibers, the experimental error is larger than for concentrations of 2% and 2.5% because the induced birefringence decreases with decreasing concentration, which results

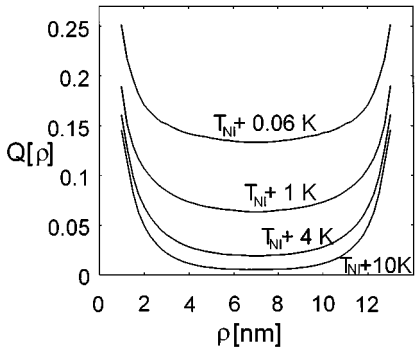

FIG. 8. Order parameter profile in a diagonal direction of a square array of parallel fibrils with radius 1 nm and interfibril distance 8.9 nm for several temperatures. The parameters of the model are the same as in Fig. 7.

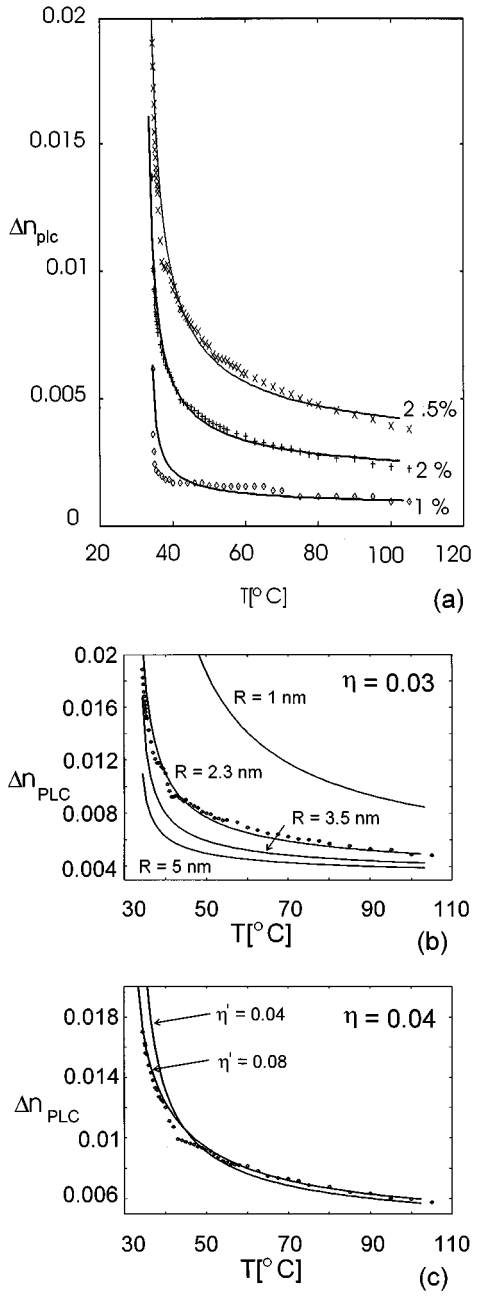

FIG. 9. Calculated birefringence using the numerical solution of Eq. (16) (line) is compared with the experimental data (dots) for various temperatures and various concentrations of the polymer network. Constants $G=0.011$ J/m^2 and $Q_n=0.5$ are equal for all concentrations. (a) For $\eta=0.025$, 0.02, and 0.01 the radius of the polymer fibers corresponding to the best fit within a one-scale model depends on the polymer concentration and is equal to 2.2, 2, and 1.8 nm, respectively. (b) For the polymer concentration 0.03, it is shown how sensitive the fit is to the variation of the radius within a one-scale model. The best fit yields $R=2.3$ nm. (c) For the $\eta=0.04$ case, the comparison of the fits obtained by one- and two-scale models is presented. The fit with the one-scale model ($\eta'=\eta$) yields $R=2.4$ nm and the fit with the two-scale model gives $\eta'=2\eta$ and $R=1.5$ nm.

in a higher uncertainty of the data. Therefore, it is not surprising that the calculated birefringence at 1% does not fit the experimental data as well as it does for higher concentrations. Figure 9(b) clearly shows how sensitive the fit is to

the change of the fibril radius. The values for a good fit are approximately twice as large as the ones obtained for BAB [2] and approximately equal to one half of the preliminary estimate performed by Fung *et al.* [32]. Figure 9(c) shows the fit for 4% polymer concentration performed with one-scale and two-scale models. In this higher concentration case, the single-scale model does not allow a very good fit while a two-scale model provides a very good fit with $R=1.5$ nm and $\eta'=2\eta$. Therefore, with our choice for the bundle thickness, we estimate the interbundle distance to be approximately 0.1 μm. The relatively large polymer–liquid-crystal coupling constant G [15] indicates that the induced liquid crystalline order parameter at the polymer surface is weakly temperature dependent, which is consistent with the findings of the NMR relaxation study [27]. Altogether, we can conclude that our visualization of the polymer network morphology describes reasonably well all experimental evidence.

VII. CONCLUSION

In our work, the ordering of a nematic liquid crystal surrounded by polymer fibrils is studied. The fibrils are locally approximated by linear rods, which are parallel and homogeneously ordered. On a larger scale, orientational and spacial inhomogeneities, characterized by macro order parameter and bundles of fibrils, are allowed.

The ordering of the liquid crystal was calculated on the basis of minimization of the Landau–de Gennes expression for the free-energy density. The birefringence of the structure composed of the polymer network and nematic liquid crystal in the isotropic phase is estimated. The calculated temperature dependence of the birefringence is compared with the experimental data. Since the agreement is very good, we may conclude that polymer networks in these samples are well described by the proposed model. The thickness of the basic building block of the network—the thin polymer fibril—is estimated to be around 4 nm. This is our main conclusion, indicating very fine distribution of polymer networks. It is comparable to the preliminary studies [2,31]. Although there are several indications that network distribution in space is nonuniform, our approach is able to indirectly ''detect'' bundles only in the 4% case, where the polymer fibril concentration in bundles is estimated to be equal to approximately twice the average value. For the networks formed in the ordered nematic liquid crystal, the macro order parameter is estimated to be between 0.3 and 0.5.

ACKNOWLEDGMENTS

This research was supported by the National Science Foundation (ALCOM Grant No. DMR 89-20147 and U.S.-Slovene Project No. 95-457) and the Ministry of Science and Technology of Slovenia (Grant No. J1-7470/790-96).

[1] G. P. Crawford, R. D. Polak, A. Scharkowski, L.-C. Chien, S. Žumer, and J. W. Doane, J. Appl. Phys. **75**, 1968 (1994).
[2] G. P. Crawford, A. Scharkowski, Y. K. Fung, J. W. Doane, and S. Žumer, Phys. Rev. E **52**, R1273 (1995).
[3] A. Jakli, L. Bata, K. Fodor-Csorba, L. I. Rosta, and L. Noirez, Liq. Cryst. **17**, 227 (1994).
[4] R. A. M. Hikmet and R. Howard, Phys. Rev. E **45**, 2752 (1993).
[5] S. C. Jain and H.-S. Kitzerow, Appl. Phys. Lett. **64**, 2946 (1994).
[6] R. A. M. Hikmet, J. Appl. Phys. **68**, 4406 (1990).
[7] D.-K. Yang, L.-C. Chien, and J. W. Doane, Appl. Phys. Lett. **60**, 3102 (1992).
[8] J. L. West, R. B. Akins, J. Francl, and J. W. Doane, Appl. Phys. Lett. **63**, 1471 (1993).
[9] D.-K. Yang, J. L. West, L.-C. Chien, and J. W. Doane, J. Appl. Phys. **76**, 1331 (1994).
[10] D.-K. Yang, J. W. Doane, Z. Yaniv, and J. Glasser, Appl. Phys. Lett. **64**, 1905 (1994).
[11] J. Pirš, R. Blinc, B. Marin, S. Pirš, and J. W. Doane, Mol. Cryst. Liq. Cryst. **264**, 155 (1995).
[12] P. J. Bos, J. A. Rahman, and J. W. Doane, Soc. Inf. Display Digest **XXIV**, 877 (1993).
[13] H. Hasebe, H. Takatsu, Y. Iimura, and S. Kobayashi, Jpn. J. Appl. Phys. **33**, 6245 (1994).
[14] A. Golemme, S. Žumer, D. W. Allender, and J. W. Doane, Phys. Rev. Lett. **61**, 1937 (1988).
[15] G. P. Crawford, R. Ondris-Crawford, S. Žumer, and J. W. Doane, Phys. Rev. Lett. **70**, 1838 (1993).
[16] T. Bellini, N. A. Clark, D. D. Muzny, L. Wu, C. W. Garland, D. W. Schaefer, and B. J. Oliver, Phys. Rev. Lett. **69**, 788 (1992).
[17] X. L. Wu, W. I. Goldburg, M. X. Liu, and J. Z. Xue, Phys. Rev. Lett. **69**, 470 (1992).
[18] G. S. Iannacchione, G. P. Crawford, S. Žumer, J. W. Doane, and D. Finotello, Phys. Rev. Lett. **71**, 2595 (1993).
[19] N. A. Clark, T. Bellini, R. M. Malzbender, B. N. Thomas, A. G. Rappaport, C. D. Muzny, D. W. Schaefer, and L. Hrubesh, Phys. Rev. Lett. **71**, 3505 (1993).
[20] A. Maritan, M. Cieplak, T. Bellini, and J. R. Banavar, Phys. Rev. Lett. **72**, 4113 (1994).
[21] P. Mariani, B. Samori, A. S. Angeloni, and P. Ferruti, Liq. Cryst. **5**, 1477 (1986).
[22] R. A. M. Hikmet, Liq. Cryst. **9**, 405 (1991).
[23] Y. K. Fung, Ph.D. dissertation, Kent State University, 1996.
[24] R. A. M. Hikmet and B. H. Zwerver, Liq. Cryst. **10**, 835 (1991).
[25] R. Stannarius, G. P. Crawford, L.-C. Chien, and J. W. Doane, J. Appl. Phys. **70**, 135 (1991).
[26] A. Jakli, D. R. Kim, L.-C. Chien, and A. Saupe, J. Appl. Phys. **72**, 3161 (1992).
[27] M. Vilfan, G. Lahajnar, I. Župančič, S. Žumer, R. Blinc, G. P. Crawford, and J. W. Doane, J. Chem. Phys. **103**, 8726 (1995).
[28] G. P. Crawford and S. Žumer, in *Liquid Crystals in Complex Geometries: Formed by Polymer and Porous Networks*, edited by G. P. Crawford and S. Žumer (Taylor & Francis, London, 1996).
[29] P. Sheng, Phys. Rev. A **26**, 1610 (1982).
[30] T. Moses and Y. R. Shen, Phys. Rev. Lett. **67**, 2033 (1991).
[31] D.-K. Yang, L.-C. Chien, and Y. K. Fung in *Liquid Crystals in*

Complex Geometries: Formed by Polymer and Porous Networks (Ref. [28]).
[32] Y. K. Fung, D.-K. Yang, S. Ying, L.-C. Chien, S. Žumer, and J. W. Doane, Liq. Cryst. **19**, 797 (1995).
[33] P. G. de Gennes and J. Prost, *The Physics of the Liquid Crystals* (Clarendon, Oxford, 1993).
[34] S. Žumer, Phys. Rev. A **37**, 4006 (1988).
[35] S. Žumer, A. Golemme, and J. W. Doane, J. Opt. Soc. Am. A **6**, 403 (1989).
[36] P. Sheng in *Introduction to Liquid Crystals*, edited by E. B. Priestley and P. J. Wojtowicz (Plenum, New York, 1974).
[37] H. J. Coles, Mol. Cryst. Liq. Cryst. **49**, 67 (1978).
[38] M. Nobili and G. Durand, Phys. Rev. A **46**, R6174 (1992).
[39] A. Borštnik, diploma thesis, University of Ljubljana, 1995.